PHYSICAL REVIEW A VOLUME 60, NUMBER 4 OCTOBER 1999

Polarization-dependent Rabi frequency beats in the coherent response of Tm^{3+} in YAG

C. Greiner, B. Boggs, T. Loftus, T. Wang, and T. W. Mossberg
Oregon Center for Optics and Department of Physics, University of Oregon, Eugene, Oregon 97403
(Received 12 July 1999)

We experimentally and theoretically investigate the coherent response of Tm^{3+} ions in yttrium aluminum garnet (YAG). Working on the $^3H_6(1)\rightarrow{}^3H_4(1)$ transition we observe optical nutation signals that exhibit multiple distinct Fourier components having polarization-dependent frequencies and weights. This phenomenon is caused by the presence of six different transition-dipole moment orientations of Tm^{3+} ions in YAG and a resultant dependence of ion-field coupling on field-propagation direction and polarization. Experimental data shown are in excellent agreement with simulation results based on numerical integration of the Maxwell-Bloch equations. [S1050-2947(99)51810-6]

PACS number(s): 42.50.Md, 42.65.−k

A two-level atom responds to a coherent resonant step-function light pulse by executing Rabi oscillations back and forth between its ground and excited states. Associated with the population oscillation is an induced dipole moment that reacts back on the driving field and causes it to be amplitude modulated at the frequency of the Rabi oscillations. This phenomenon is referred to as optical nutation and is analogous to the nuclear magnetic transient effect [1]. Nutation can be observed in the transmission through a sample whenever the Rabi period is comparable to or shorter than the homogeneous atomic dephasing time. Since its first observation in 1968 [2], optical nutation has been extensively used in the study of two [3] and multilevel atomic dynamics [4], has been employed to probe dressed atomic systems [5], and has been a useful tool in the measurement of spectroscopically important parameters such as transition dipole moments [6]. Time-reversed optical nutation signals allow the study of homogeneous relaxation processes otherwise obscured by inhomogeneous line broadening [7]. While the first observation of optical nutation involved a *Q*-switched laser to create the excitation pulse, alternative experimental techniques employed Stark pulses to shift molecular transitions into resonance with an applied cw laser [8] or frequency switchable lasers [9].

Simple treatments of this fundamental light-matter interaction commonly posit a single resonant Rabi frequency as a coupling parameter, a simplification that cannot be regarded as a general rule. When the interacting ions are embedded in crystalline materials transition dipole moments can assume different spatial orientations owing to the presence of multiple nonequivalent crystal sites. In this case, the orientational dependence of the Rabi frequency as implied in the scalar product between electric field and transition dipole moment can lead to multivalued ion-field coupling and the occurrence of frequency beats between the Rabi oscillations of ions located on different sites. This phenomenon is not only of fundamental interest, it may also provide a means to determine the relative spatial orientations of the contributing transition-dipole moments.

In this paper we present a study of how the presence of multiple transition dipole-moment orientations impacts optical coherent transients. Specifically, we show how the six different $^3H_6(1)\rightarrow{}^3H_4(1)$ transition-dipole moment orientations of Tm^{3+} in yttrium aluminum garnet (YAG) manifest themselves in optical nutation signals. Tm^{3+}:YAG is a material of technological importance not only as a laser crystal, but has also been used in the demonstration of signal-routing and data-storage techniques based on coherent transients [10]. Site-symmetry-induced polarization effects in the context of *Q*-switched Nd:YAG laser operation have been recently reported in Ref. [11].

We remark that multiple values for the resonant Rabi frequency can also occur in multilevel excitation schemes wherein the levels involved exhibit magnetic degeneracy [12]: This is due to the fact that the relative orientation between the transition dipole moment and the electric field depends on the magnetic quantum number as expressed in the Clebsch-Gordan coefficient. A further consequence of a Rabi frequency distribution is the nonexistence of pulse flipping angles with well-defined area, as was pointed out in Ref. [13].

Figure 1 is a schematic of the experimental setup. Excitation pulses are obtained by acousto-optically gating a single-mode cw Ti:sapphire laser. The first-order diffracted beam of the acousto-optic modulator (rise time ~100 ns) is linearly polarized by a Glan-Taylor polarizing prism. It passes through a rotatable half-wave plate and is subsequently focused along the axis of the cylindrically shaped Tm^{3+}:YAG crystal. The measured ellipticity of the input-field polarization is less than $E_2/E_1\approx 2\times 10^{-2}$, where E_2 is the electric-field strength in the direction perpendicular to the direction of maximum field strength E_1. Experiments are conducted at a sample mount temperature of ~3.3 K. The focal spot in the crystal (calculated $1/e^2$ diameter ~140 μm) is imaged with a magnification of ~2.6 onto a 25-μm-diam pinhole (aligned for maximum transmission) to limit observed transverse excitation-field variations to an estimated 1%. The transmit-

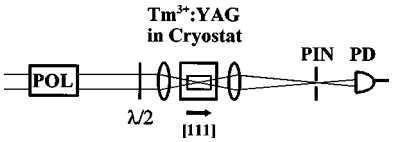

FIG. 1. Schematic diagram of the experimental setup. POL, Glan-Taylor polarizing prism; PD, photodiode; λ/2, half-wave plate; PIN, pinhole. The arrow indicates the [111] direction in the crystal.

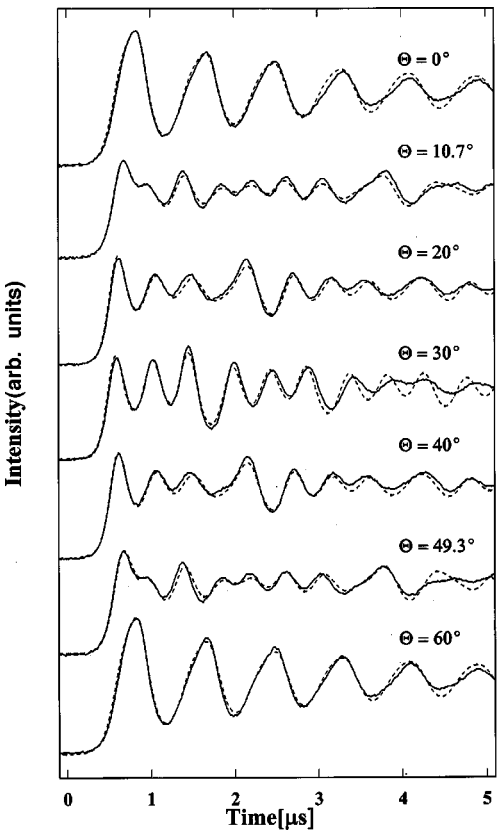

FIG. 2. Optical nutation signals. Solid lines, experimental data; dashed lines, simulation results. Θ values refer to the orientation of the electric field's linear polarization in the simulation.

ted signal is detected by a 50-MHz photodiode-amplifier combination and subsequently observed and stored on a digital storage oscilloscope.

The 0.5 at. % Tm^{3+}:YAG sample has a diameter of 3 mm, a length $L \approx 7$ mm, and is cut such that the cylinder axis and hence the excitation direction is parallel to the [111] direction of the crystal. The output end of the crystal is cut with its normal 6° away from the cylinder axis to prevent reflected light from introducing standing-wave variations in excitation intensity. The ${}^3H_6(1) \rightarrow {}^3H_4(1)$ transition employed in our experiment has an inhomogeneous linewidth of ~18 GHz at a temperature of 4.2 K and an optical thickness of $\alpha L \approx 5.4$ at the wavelength (in air) used in the experiment, $\lambda_{air} \approx 793.16$ nm. Note that the crystal's high optical thickness can cause substantial axial variation in the excitation-field magnitude.

In Fig. 2 we present experimentally obtained optical nutation signals (solid lines). The data shown were generated by monitoring the transmission of a 10-μs-long 400-mW square pulse through the sample. In the graph, $t=0$ refers to the beginning of the pulse. The half-wave plate was used to rotate the input-field polarization. From the top to the bottom of Fig. 2, successive traces correspond to increments of ~10° in the direction of electric-field polarization. The Θ values shown refer to the input parameter for the electric-field orientation in a computer simulation described in later paragraphs. The experimentally observed optical nutation signal exhibits interesting behavior in that it evolves from a single-frequency oscillation (top trace of Fig. 2) to more complex shapes containing oscillations at multiple frequencies. Intriguingly, the shape of the nutation signals at 0°, 10.7°, and 20° is reproduced at 60°, 49.3°, and 40°, respectively. Our observations can be explained on the premise of different spatial orientations of the Tm^{3+} transition dipole moments in YAG. In order to attain a complete understanding of the observed nutation signal shapes and symmetry we develop a theoretical model based on the geometry of the Tm^{3+} sites in YAG and numerical integration of the Maxwell-Bloch equations.

Yttrium aluminum garnet (YAG) has the chemical composition $Y_3Al_5O_{12}$ and the cubic space-group symmetry $O_h^{10}(Ia3d)$ with eight formula units per unit cell [14]. Tm^{3+} ions substitute for Y^{3+} ions on the dodecahedral sites and experience a crystal field of D_2 symmetry [15]. The six differently oriented Tm^{3+} sites are represented in Fig. 3(a) (after Ref. [16]) by matchboxes, whose shape is symbolic of the crystal field's D_2 symmetry at the Tm^{3+} sites. The local axes of the Tm^{3+} site are oriented along the [110], [$1\bar{1}0$], and

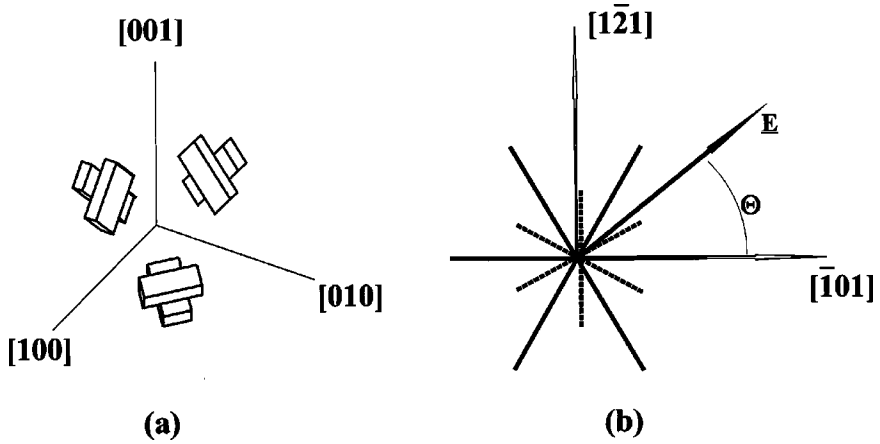

FIG. 3. (a) Orientations of the six Tm^{3+} sites relative to the axes of the cubic unit cell of YAG (after Ref. [16]). (b) Projections of the ${}^3H_6(1) \rightarrow {}^3H_4(1)$ transition-dipole moments in the plane perpendicular to the [111] direction. Dipole moment projections represented by dashed (solid) lines correspond to transition-dipole moments that make an angle of 35.3° (90°) with the [111] direction.

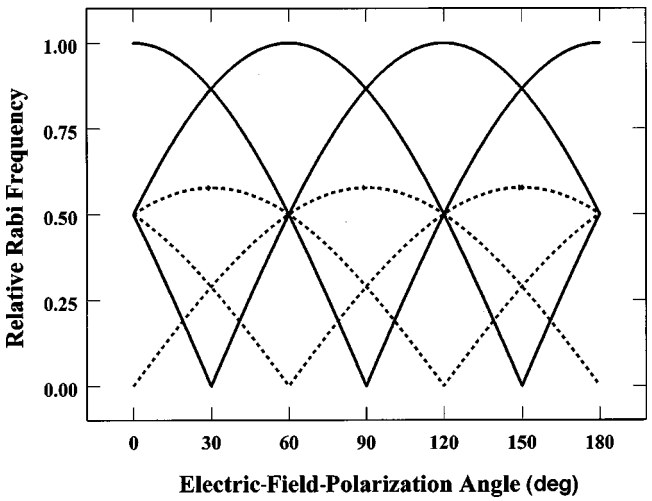

FIG. 4. Relative Rabi frequencies versus electric-field polarization angle Θ. We define $\Theta = 0°$ when the electric field is parallel to the $[\bar{1}01]$ direction.

[001] crystal axes and the six equivalent directions. Following Ref. [17] we take the local *x*, *y*, and *z* axes of the Tm^{3+} sites parallel to the longest, the intermediate, and the shortest dimensions of the matchboxes in Fig. 3(a). The transition dipole moment of the electric-dipole transition between the lowest Stark level of the Tm^{3+} ground state $^3H_6$ and the lowest Stark level of the $^3H_4$ manifold is oriented along the *y* axis of the Tm^{3+} site [15]. In the coordinate system of the cubic YAG unit cell the local *y* axes of the Tm^{3+} sites correspond to the directions of the six face diagonals.

In Fig. 3(b) we show the projections of the six $^3H_6(1) \rightarrow {}^3H_4(1)$ transition dipole moments in the plane perpendicular to the [111] direction, i.e., perpendicular to the direction of light propagation. Dipole-moment projections fall into two categories represented by dashed and solid lines. Dashed (solid) lines correspond to dipole moments that are angled at 35.3° (90°) with the [111] direction. While elements within each category are angled at 120° with respect to each other, they make angles of 30° with the components of the other category. The resulting relative Rabi frequencies for light propagation along the [111] direction are shown in Fig. 4 as a function of the angle Θ that the electric-field vector makes with the $[\bar{1}01]$ direction. The distribution of Rabi frequencies exhibits even symmetry about $\Theta = m*30°$, where $m = 0,1,2,\ldots$. Note that for $\Theta = m*60°$ the Rabi frequencies for four out of the six sites become degenerate. Looking at Fig. 4 it is reasonable to expect that the symmetry of the Rabi frequencies should manifest itself in the optical nutation signal. We examine this hypothesis in the following by numerically modeling the transmitted intensity of an excitation pulse as a function of the direction of input-field polarization with respect to the crystal axes.

Our simulation is based on the numerical integration of the Maxwell-Bloch equations [18]. The physical system used for modeling consists of an ensemble of inhomogenously broadened two-level atoms and linearly polarized collimated excitation pulses with a rectangular transverse intensity profile that propagate along the [111] direction of the crystal, taken to be the $+z$ direction. Atoms are located on equidistant positions on the $z \geqslant 0$ axis that correspond to optically thin ($\alpha L = 0.06$) layers of absorbers. For each layer there are six equally populated sites with transition-dipole-moment orientations, as shown in Fig. 3(b). Simulations are carried out as follows: At the input face of the first layer, the input electric field is projected onto each of the transition-dipole moments. Using the projected electric field, the atomic polarization at each of the crystal sites is calculated as described in Ref. [18]. For ions at subsequent *z* positions the field is equal to the input field plus the fields generated by the electric dipoles of all the atoms at previous positions. Note that the spatial orientations of the transition dipole moments introduce a field component transverse to the original input field, thereby effectively causing a position- and time-dependent rotation of the electric field. The results of our simulation are shown as dashed lines in Fig. 2. As input parameters to the simulation we use a 10-μs-long square pulse with a Rabi frequency of 2.5 MHz for dipole moments aligned parallel to the electric field, an inhomogeneous linewidth of 40 MHz (full width at half maximum), an excited-state lifetime T_1 of 1 ms, and set the atomic dephasing time T_2 to 6 μs, consistent with experimentally obtained values for T_1 and T_2. Θ values given in Fig. 2 refer to the orientation of the electric field in the simulation. Transmitted intensities shown correspond to the output side of the sample at $\alpha L = 5.4$. As can be seen in Fig. 2, simulation results and experimental data are in excellent agreement, therefore confirming that the shape and symmetry of the nutation signals in Fig. 2 are caused by the geometry of the Tm^{3+} transition dipole moments in YAG.

An additional point of interest in the data of Fig. 2 merits our attention. It is the apparent single-frequency oscillation of the $\Theta = 0°$, 60° traces. This single-frequency behavior comes as a surprise, as, based on Fig. 4, a second faster frequency component at 2.5 MHz—caused by a Tm^{3+} site that has a transition dipole moment parallel to the input field—would be expected. The 2.5-MHz component is in fact observed in simulations with samples of low optical thickness ($\alpha L \ll 1$). However, when we increase the optical thickness of the sample beyond $\alpha L \approx 5$ and observe the reradiated field of this parallel site at the output face, it exhibits a slow amplitude modulation at one-half of the value of the input face Rabi frequency. This spectral distillation of the parallel site's nutation frequency to a subharmonic of the input face Rabi frequency is caused by the absorber-mediated modifications to the input field and will be the subject of future, more detailed investigations.

In summary, we observe Rabi frequency beats in the nutation signals of Tm^{3+} in YAG that depend on the orientation of the input field's linear polarization relative to the crystal axes. This effect is explained in terms of the six different Tm^{3+} sites and hence $^3H_6(1) \rightarrow {}^3H_4(1)$ transition dipole-moment orientations found in YAG. Experimentally observed nutation signals agree well with theoretical results based on integration of the Maxwell-Bloch equations. The polarization dependence of the frequency content of the nutation signals and especially the presence of reradiated field components in the direction transverse to the input field may lead to a useful spectroscopic method for site identification.

Further investigations will also include the effect of crystal site geometry on parameters relevant in coherent-transient based signal routing and data storage; e.g., photon-echo power efficiency.

The authors wish to thank Randy Equall of Scientific Materials for helpful comments. We appreciate support from Dr. Alan Craig and the U.S. Air Force Office of Scientific Research under Contract No. F49620-96-1-0259.

[1] H. C. Torrey, Phys. Rev. **76**, 1059 (1949).
[2] G. B. Hocker and C. L. Tang, Phys. Rev. Lett. **21**, 591 (1968).
[3] L. Allen and J. H. Eberly, *Optical Resonance and Two-Level Atoms* (Dover, New York, 1987), and references therein.
[4] Y. Zhu, J. Opt. Soc. Am. B **14**, 2596 (1997), and references therein; M. M. T. Loy, Phys. Rev. Lett. **36**, 1454 (1976).
[5] Q. Wu, D. J. Gauthier and T. W. Mossberg, Phys. Rev. A **50**, 1474 (1994); C. Wei, N. B. Manson, and John P. D. Martin, Phys. Rev. Lett. **74**, 1083 (1995).
[6] G. B. Hocker and C. L. Tang, Phys. Rev. **184**, 356 (1969); R. L. Shoemaker and E. W. Van Stryland, J. Chem. Phys. **64**, 1733 (1976).
[7] Y. S. Bai, A. G. Yodh, and T. W. Mossberg, Phys. Rev. A **34**, 1222 (1986).
[8] R. G. Brewer and R. L. Shoemaker, Phys. Rev. Lett. **27**, 631 (1971).
[9] R. G. Brewer and A. Z. Genack, Phys. Rev. Lett. **36**, 959 (1976).
[10] T. Wang, H. Lin, and T. W. Mossberg, Opt. Lett. **20**, 2541 (1995); H. Lin, T. Wang, and T. W. Mossberg, *ibid.* **20**, 1528 (1995).
[11] M. Lukač, S. Trošt, and M. Kažič, IEEE J. Quantum Electron. **28**, 2560 (1992); P. Esherick and A. Owyoung, Proc. SPIE **912**, 2 (1988).
[12] B. W. Shore, Phys. Rev. A **17**, 1739 (1978); A. Kastberg, P. Villemoes, A. Arnesen, F. Heijkenskjöld, A. Langereis, P. Jungner, and S. Linnaeus, Opt. Commun. **101**, 25 (1993); A. Wännström, A. Kastberg, A. Arnesen, R. Hallin, C. Nordling, O. Vogel, and S. Linnaeus, Phys. Rev. A **41**, 440 (1990).
[13] W. S. Warren, J. L. Bates, M. A. McCoy, M. Navratil, and L. Mueller, J. Opt. Soc. Am. B **3**, 488 (1986).
[14] S. Geller, Z. Kristallogr. **125**, 1 (1967).
[15] J. B. Gruber, M. E. Hills, R. M. Macfarlane, C. A. Morrison, G. A. Turner, G. J. Quarles, G. J. Kintz, and L. Esterowitz, Phys. Rev. B **40**, 9464 (1989).
[16] J. F. Dillon, Jr. and L. R. Walker, Phys. Rev. **124**, 1401 (1961).
[17] J. P. Van der Ziel, M. D. Sturge, and L. G. Van Uitert, Phys. Rev. Lett. **27**, 508 (1971).
[18] T. Wang, C. Greiner, and T. W. Mossberg, Opt. Commun. **153**, 307 (1998).